Sliding-induced adhesion of stiff polymer microfibre arrays. I. Macroscale behaviour

Jongho Lee[1],[*], Carmel Majidi[2], Bryan Schubert[2] and Ronald S. Fearing[2]

[1]*Department of Mechanical Engineering, and* [2]*Department of Electrical Engineering and Computer Sciences, University of California, Berkeley, CA 94720, USA*

Gecko-inspired microfibre arrays with 42 million polypropylene fibres cm^{-2} (each fibre with elastic modulus 1 GPa, length 20 μm and diameter 0.6 μm) were fabricated and tested under pure shear loading conditions, after removing a preload of less than 0.1 N cm^{-2}. After sliding to engage fibres, 2 cm^2 patches developed up to 4 N of shear force with an estimated contact region of 0.44 cm^2. The control unfibrillated surface had no measurable shear force. For comparison, a natural setal patch tested under the same conditions on smooth glass showed approximately seven times greater shear per unit estimated contact region. Similar to gecko fibre arrays, the synthetic patch maintains contact and increases shear force with sliding. The high shear force observed (approx. 210 nN per fibre) suggests that fibres are in side contact, providing a larger true contact area than would be obtained by tip contact. Shear force increased over the course of repeated tests for synthetic patches, suggesting deformation of fibres into more favourable conformations.

Keywords: bio-inspired adhesion; gecko; friction; shear; sliding

1. INTRODUCTION

Natural geckos have exceptional wall-climbing ability using their millions of micro/nano fibrillar structures. The gecko's keratin fibre arrays form a unique attachment mechanism that is non-adhesive by default (Autumn & Hansen 2006), but can be easily engaged with low compressive preload and sliding to develop high shear force (Autumn *et al.* 2000), and controllably released with low pull-off force (Gravish *et al.* 2008). These properties of the natural gecko are critical for efficiently and reliably running up walls. In characterizing the behaviour of a 'directional' adhesive, we refer to the tensile force (normal to a surface) and the shear force (parallel to a surface). It is important to note that the tensile and shear forces can be strongly coupled and may depend on both compressive preload (normal to surface) and engagement trajectories. In this paper, we examine the macroscale behaviour of a synthetic gecko patch. As the whole patch is non-adhesive by default in the normal direction, the patch is tested under pure shear loading, where forces are constrained to be parallel to a surface.[1] Under shear loading, membrane buckling effects dominate behaviour. In part II of this paper, Schubert *et al.* (2008) examine a microscale spherical indentation of a synthetic gecko patch that is

fixed to a backing layer to avoid membrane buckling effects. Under combined shear and normal loading the patch demonstrates a *frictional adhesion* effect, whereby a normal tensile load can be supported only under conditions of an applied shear load.

There is an increasing interest by researchers in understanding and fabricating gecko-inspired synthetic adhesives (GSAs; Autumn 2007; Autumn & Gravish 2008) using materials that range in hardness from soft polymers to carbon nanotubes ($E \sim 3 \times 10^5$–10^{12} Pa). Harder materials allow greater fibre packing density (Sitti & Fearing 2003), and probably better resist wear and particle contamination. Recent work using soft polymer fibre arrays (Kim & Sitti 2006; Gorb *et al.* 2007; Santos *et al.* 2007) has increased normal adhesion several times over the bulk material. Multiwalled carbon nanotubes (MWCNT; Zhao *et al.* 2006; Ge *et al.* 2007) and low aspect ratio (length/diameter = 0.5–10) hard polymer stalks (Geim *et al.* 2003) demonstrated tensile adhesion but they require high normal compressive preload. Kustandi *et al.* (2007) have recently demonstrated 0.7 N cm^{-2} tensile adhesion with preload pressure of 1 N cm^{-2} using 10 : 1 aspect ratio hard polymer fibres ($E \sim 2.8$ GPa).

Fibre arrays have also demonstrated high friction forces (i.e. high shear forces with normal compressive loads which engage fibres) such as Majidi *et al.* (2006) with coefficient of friction $\mu > 5$ using polypropylene (PP) and Aksak *et al.* (2007b) with $\mu > 1$ using MWCNT. In these examples the shear force required a sustained normal compressive load and the samples did not show shear or tensile adhesion.

---

*Author for correspondence (jongho@eecs.berkeley.edu).

[1]Pure shear loading with zero normal load or peeling moment was also used by Zhao *et al.* (2006) and Ge *et al.* (2007) to test patch behaviour, and is well known in material testing (e.g. Antoniou & Bastawros 2003).
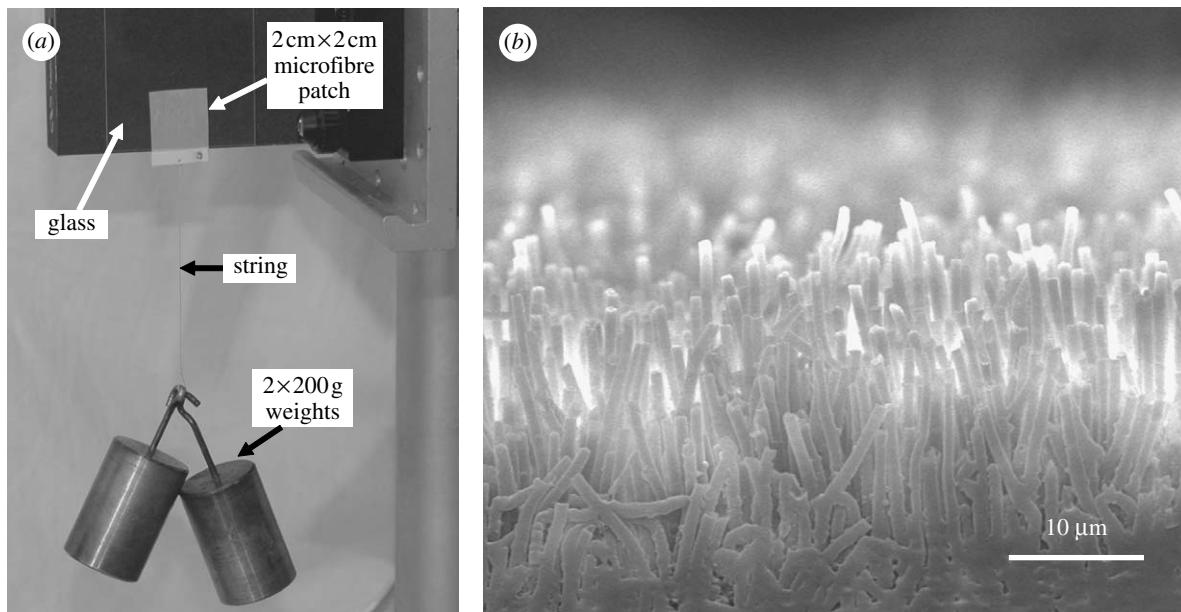
Electronic supplementary material is available at http://dx.doi.org/10.1098/rsif.2007.1308 or via http://journals.royalsociety.org.

Figure 1. (*a*) A $2\times2\,\text{cm}^2$ microfibre array patch holding two 200 g weights (400 g) on a vertical smooth glass slide without normal load. (*b*) A scanning electron microscopy (SEM) image of a microfibre array. Average length and diameter of the microfibres are 18 μm and 0.6 μm, respectively.

To simultaneously obtain high shear force and low tensile pull-off forces with a low initial compressive preload, we have designed an array of microfibres that makes side contact with a surface (Majidi *et al.* 2005). In contrast, structures such as those of Geim *et al.* (2003) and Kustandi *et al.* (2007) use tip contact of fibres. We fabricated an array of 0.6 μm diameter PP fibres whose elastic modulus ($E\sim1$ GPa) and aspect ratio (approx. 30) are similar to natural tokay gecko setae with $E\sim1.5$ GPa (Autumn *et al.* 2006*a*; Peattie *et al.* 2007) and aspect ratio approximately 25 (Ruibal & Ernst 1965). In contrast to Majidi *et al.* (2006), these patches were fabricated with reduced backing curvature to enable fibre engagement without sustained compressive normal loading. (The important effect of backing curvature on adhesion is discussed in Schubert *et al.* (2007).) The flat backing samples with millions of microfibres show shear adhesion as demonstrated in figure 1*a*.

In this paper, we first directly compare the stiff polymer-based microfibre adhesive to a natural gecko setal array under pure shear loading. The high elastic modulus material and vertical fibres in figure 1*b* make the fibre array intrinsically non-adhesive by default. (Angled fibres as suggested by Sitti & Fearing (2003) could be used to have an initially adhesive state.) We show experimentally that high shear adhesion can be induced by sliding displacement alone with minimal initial normal compressive preload, but can be easily detached in the normal tensile direction (low 90° peel strength). We also show that the adhesion demonstrated in figure 1*a* does not depend on an internal viscoelastic property. Durability of some previous GSAs has been a problem (e.g. Zhao *et al.* 2006). Tests of the PP microfibre array showed an increase in shear adhesion force with repeated uses. In §4, we demonstrate that the measured shear stress in the estimated contact region of 9 N cm^{-2} is consistent with fibres in side contact with the surface.

2. MATERIAL AND METHODS

2.1. Material preparation

GSA samples were fabricated by casting a single layer of 25 μm thick PP (TF-225-4, Premier Lab Supply, Inc.) in a vacuum oven at 200°C into a 20 μm thick polycarbonate filter (ISOPORE, Millipore, Inc.) containing 0.6 μm diameter pores. The polycarbonate filter was etched in methylene chloride, and resulting samples were rinsed in isopropyl alcohol and air-dried. Backing curvature was significantly reduced when compared with the previous microfibre arrays (Majidi *et al.* 2006), increasing the number of fibres in contact and adhesion. Using a fixed fibre length, the fibre diameter was selected to provide enough compliance while preventing fibres from clumping. Control measurements were performed on processed 25 μm thick PP film that underwent the same fabrication steps as the fibre arrays, with the exception that no polycarbonate filter was applied. Both the microstructured samples and controls were cut into $2\times2\,\text{cm}^2$ squares. For some samples that demonstrated higher shear force than the limit of the force sensor, smaller areas ($2\times1.2\,\text{cm}^2$ and $2\times0.8\,\text{cm}^2$) were used.

Natural gecko setal arrays were prepared by N. Gravish, M. Wilkinson and K. Autumn in the Department of Biology, Lewis and Clark College, Portland, OR, USA. Individual lamellae were isolated from tokay geckos. Each isolated lamella was fixed to the end of a $2.5\times0.6\times0.02\,\text{cm}^3$ acetate strip using cyanoacrylate SuperGlue Gel. The areas of gecko setal arrays tested were $0.11\times0.03\,\text{cm}^2$ and $0.18\times0.03\,\text{cm}^2$.

2.2. Measurement methods

Macroscale shear adhesion tests during sliding with no normal compressive load were performed with the single axis force sensor system in figure 2*a*. The system is composed of a stepper motor (TS Products model
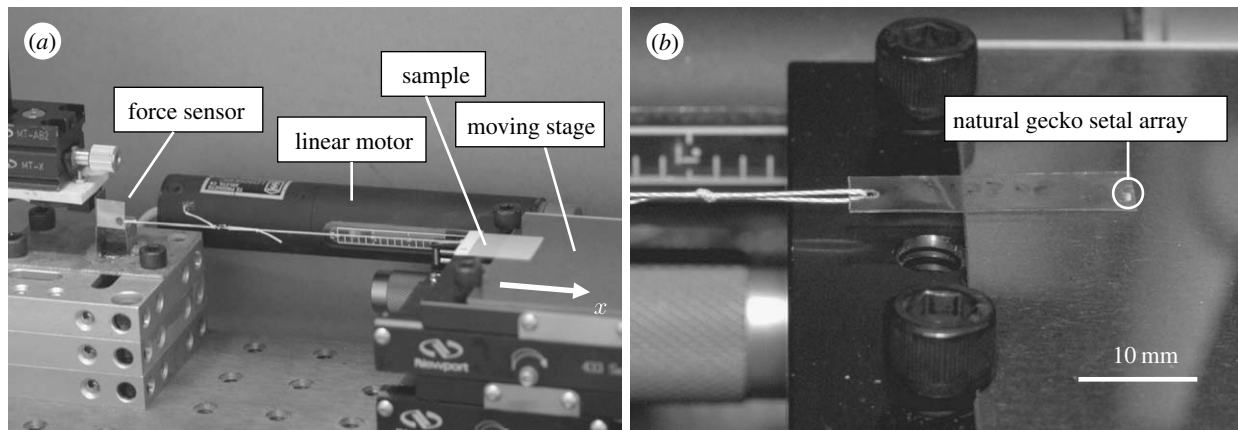
Figure 2. (*a*) Testing set-up: shear force of a 2×2 cm^2 synthetic microfibre array patch on a glass slide is being measured while the stage is driven in the x-direction by the linear motor. (*b*) Natural gecko setal array under shear load on same test set-up.

2200)-driven linear stage with a linear variable differential transformer (LVDT) position sensor (MEPTS-9000, Techkor Instrumentation) and double cantilever force sensor (Schubert *et al.* 2007). The force sensors were calibrated with known weights. The force sensor for microfibre array samples had stiffness 10^5 N m^{-1} and resolution less than 42 mN. A more sensitive force sensor (stiffness 3×10^4 N m^{-1}, resolution less than 13 mN) was used for natural gecko setal arrays.

Each sample was connected to a force sensor using a string (Kevlar, Dupont) and was placed on a glass slide (Microscopes slides, Fisher Scientific) on top of the stage. The glass slide had surface roughness (root mean square (r.m.s.) = 3.3 nm, see electronic supplementary material) and was cleaned using isopropanol to remove dust before using. Before shear testing, a normal preload pressure (less than 0.1 N cm^{-2}) was applied by gloved finger to remove any possible initial curvature of the backing. A separate test showed that the preload used had a negligible effect on shear force. After the preload was removed, the stage was driven at constant speeds which ranged from 48 to 240 μm s^{-1} in the x-direction in figure 2a. During testing, the normal stress due to weight of the patch was less than 0.3 mN cm^{-2}. This normal stress is not needed to sustain shear stress as can be seen in figure 1a. The gecko setal array under testing is shown in figure 2b. While driving the stage, shear force and stage displacement were recorded by a four-channel digital oscilloscope (TDS3014B, Tektronix).

Estimated contact region of samples was recorded by a camcorder (DCR-TRV520, Sony) using reflected white light through the back of the sample. This estimated contact region represents regions where fibres may be touching the glass substrate. Owing to the backing membrane roughness, all fibres in the bright region are not necessarily touching the glass.

3. RESULTS

For both the microfibre array and natural gecko, shear force increased with sliding distance. The microfibre sample continued to function after 50 pure shear tests. In addition to durability, repeated sliding tests showed increase of maximum shear force of microfibre array samples.
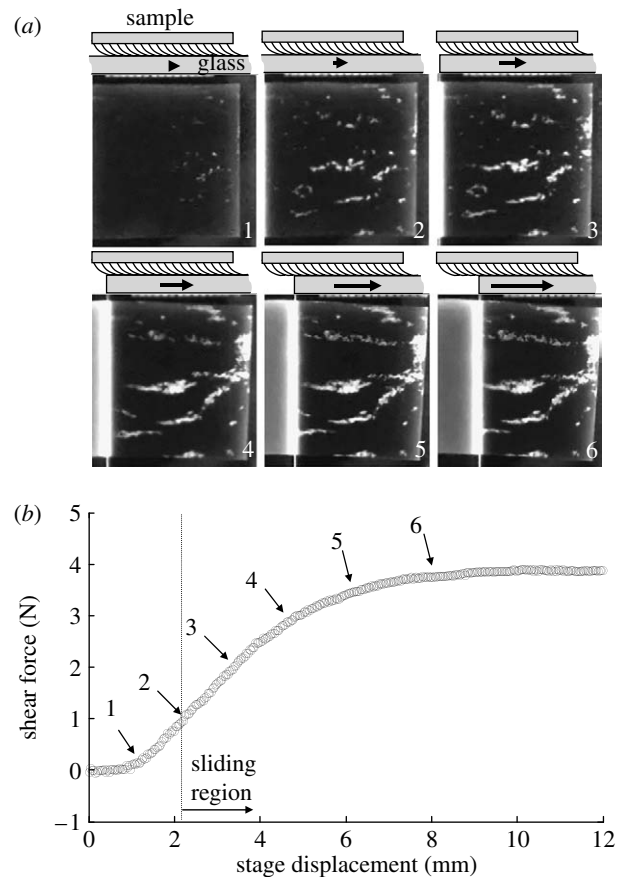

Figure 3. Shear force of a 2×2 cm^2 synthetic microfibre array with zero normal load increased monotonically during tangential displacement (stage velocity $V_x = 120$ μm s^{-1}). (*a*) Estimated contact region (white amorphous regions) at indicated positions. Estimated contact region is 11% of patch area when the patch slides 1 cm, with possible buckling of membrane in dark (non-contact) regions. (*b*) Shear force increases even as patch slides off glass.

As plotted in figure 3, shear force increased as the microfibre patch was pulled on smooth glass in the tangential (x) direction with no normal load. (Pressure due to weight of patch is less than 0.3 mN cm^{-2}.) Pulling velocity for the stage was 120 μm s^{-1}. Effects of other preloads and velocities are presented later in this paper. Initially, shear force increased as the stage moved for the first several millimetres and saturated at
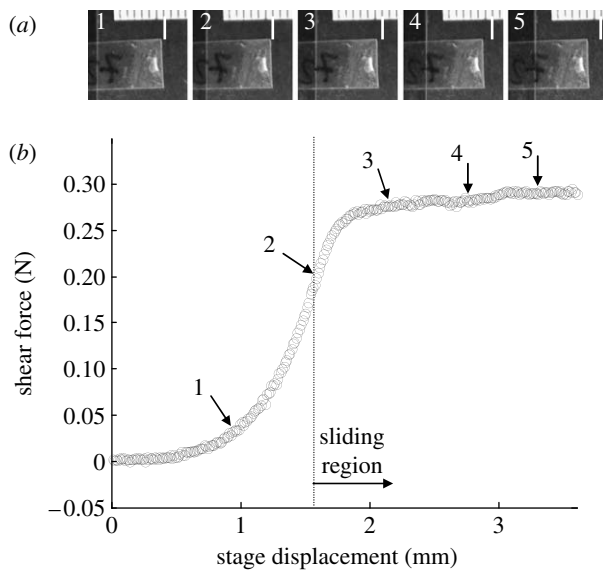
(a)

(b)

Figure 4. (*a*) Natural setal array under testing at indicated positions. The captured images indicate that the sample actually began sliding at 0.2 N due to compliance of the sensor system including the string. (*b*) Shear force of a 0.18×0.03 cm^2 natural gecko setal array with zero normal load during tangential displacement of the stage (stage velocity $V_x = 120$ μm s^{-1}).

approximately 4 N shear force. From examination of captured images, the sample did not slide until the shear force exceeded 1 N. Images 1–6 in figure 3*a* show that estimated contact region (white amorphous regions) on glass increases as the synthetic microfibre patch slides. In image 1, the square patch placed on a glass slide had only several tiny contacting points after normal preload was removed. As the glass moved to the right (images 2–6), the initial contact areas grew. Even though the sample lost some overlap area (white rectangular region in images 4–6) with the glass because the glass slid to the right, absolute shear force increased. The peak shear stress with estimated contact area fraction (white amorphous area (0.44 cm^2)/patch area (4 cm^2)) of 11% was 9 N cm^{-2}. The white amorphous estimated contact region was determined by image processing (MATLAB R2006a, The Math-Works, Inc.). The control (r.m.s. surface roughness 6.8 nm, see electronic supplementary material), unstructured PP, had no observable shear stress (less than 0.3 mN cm^{-2}). The microfibre arrays have high shear adhesion but low normal adhesion. For example, only 3 ± 0.4 mN (mean $\pm$ s.d., $N = 5$) of perpendicular force is required to peel the sample from glass. This corresponds to a 90° peel strength of 0.15 ± 0.02 N m^{-1}.

Tests with a 0.18×0.03 cm^2 natural gecko setal array with a gravitational compressive normal stress (less than 50 mN cm^{-2}) showed similar sliding-induced shear force and saturation (figure 4). No external preload was applied. Pulling velocity for the natural gecko setal array was 120 μm s^{-1}. The images 1–5 in figure 4*a* show relative position of the natural setal array and glass under testing at indicated times. The images indicate that the gecko setal array started sliding after the shear force exceeded 0.2 N, and shear force approximately saturated after 200 μm displacement.

Owing to an initially slack string, stiffness of the force sensor system including a string is nonlinear. Linearized stiffness of the system is 250 N m^{-1} for 0–0.2 N and 1600 N m^{-1} for 0.2–1.6 N. Owing to this low stiffness (250 N m^{-1}) for low load (less than 0.2 N), the gecko setal array did not slide until after 960 μm of stage movement, corresponding to 0.24 N shear force.

Velocity dependence was examined for both the synthetic adhesive and the natural gecko setal array. Both samples were pulled four times at each velocity from 48 to 240 μm s^{-1}. Average and standard deviation of plateau force are plotted in figure 5. No drastic change in shear force with velocity was seen for microfibre arrays or the natural gecko setal array.

In many GSAs (e.g. Kim & Sitti 2006; Gorb *et al.* 2007), the tensile adhesion force is a strong function of normal preload. Before shear testing, an approximately uniform preload was applied, and carefully removed before testing without disturbing the patch. A sheet of polydimethylsiloxane (PDMS) was used to distribute normal loading uniformly over a sample. A cloth (Technicloth, ITW Techwipe, Inc.) prevented soft PDMS sticking to a sample. After carefully removing this stack from a microfibre array patch, the patch was pulled at 120 μm s^{-1}. Figure 6 shows sliding-induced shear adhesion for different preloads (8–825 mN cm^{-2}), with no observable relation between preload and maximum shear force. In other tests, the microfibre array samples were gently preloaded (less than 0.1 N cm^{-2}) with a gloved forefinger for simplicity, since preload did not significantly affect maximum shear force.

Relaxation behaviour of PP microfibre arrays and the gecko setal array was significantly less than pressure sensitive adhesives (PSAs; Magic tape, Scotch, 3M) whose adhesion relies heavily on internal viscous conformation. After engaging the array by sliding, the moving stage stopped at time 0 and shear force relaxation is plotted in figure 7*a* for a synthetic microfibre array and figure 7*b* for a natural gecko setal array. After stopping, the microfibre array patch crept approximately 150 μm without leaving residue on the glass slide. Consequently, the shear force of the microfibre array decreased by 30% and then maintained a constant shear force. This experiment supports that shear adhesion of the synthetic patch does not depend on viscoelasticity of the material but sliding of microfibres on glass (§4). After stopping, as with the microfibre array, shear force of the natural gecko setal array also decreased by 20%, then maintained a constant level. In contrast to a microfibre array and natural gecko setal array, a 0.2×0.5 cm^2 PSA adhered and did not slide on glass during loading. After stopping the stage at 0 s, the PSA crept while leaving much soft polymer residue on the glass. Consequently, shear force kept decreasing as shown in figure 7*c*.

Microfibre array patches survived more than 50 high shear tests without a reduction in shear force. Instead of a reduction in force, a training effect was observed with repeated tests. As the sample was dragged repeatedly with zero normal load, maximum saturated shear force increased as shown in figure 8.
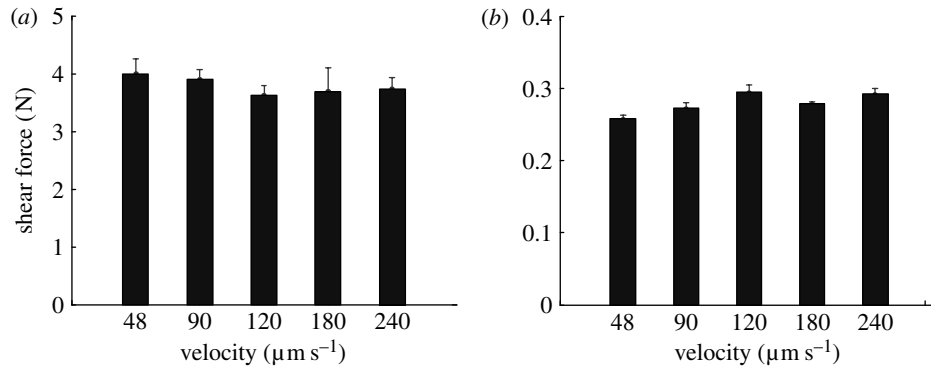
Figure 5. Maximum shear force for various velocities. Each sample was tested four times at each velocity. Patch sizes of (*a*) synthetic microfibre array and (*b*) natural gecko setal array are 2×0.8 cm^2 and 0.18×0.03 cm^2, respectively.

When shear force approached saturation, the sample sometimes slipped, presumably due to buckling of the thin backing of the patch as shown in the fifth test in figure 8. Shear force drops were also observed with natural gecko setal arrays at high load. For both materials, shear force recovered after slip events.

4. DISCUSSION

Experimental results with centimetre-sized microfibre arrays have shown several key GSA properties, including relatively strong shear adhesion with low peel strength, low normal preload for fibre engagement and durability over multiple attachment cycles. We explain the observed shear forces using a fibre side-contact model. Angling of the fibres after sliding can be observed in microscope images, and is consistent with the increase in shear adhesion with use. Finally, we compare the performance of various GSAs, and discuss how the behaviour of the PP microfibre array relates to tasks such as wall climbing.

4.1. Shear adhesion-induced side contact

The shear stress shown in figure 3 saturates at approximately 9 N cm^{-2} per unit estimated contact region. With a fibre density of $\rho = 42\times10^6$ fibres cm^{-2}, this corresponds to an average shear force of approximately 210 nN per fibre. This shear force is much higher than predicted by Johnson–Kendall–Roberts (JKR) theory (Johnson *et al.* 1971) for a spherical fibre tip.[2] For tip contact, the shear force can be estimated from $V_{\text{tip}} = \tau A_{\text{t}}$, where A_{t} is the true tip contact area and τ is the interfacial shear strength (10 MPa for PP on glass; Pooley & Tabor 1972). (Note that for hard polymers, the true contact area is very small compared with tip size.) The estimated shear force V_{tip} is only 33 nN for tip contact with $r = 0.3\times10^{-6}$ m fibre radius, $E = 1$ GPa and $W_{\text{ad}} = 30$ mJ m^{-2}, the work of adhesion of PP on glass (Gracias & Somorjai 1998).

The tip contact model underestimates the measured shear force by a factor of 6. However, we observe that the measured shear force on the fibres is high enough to cause
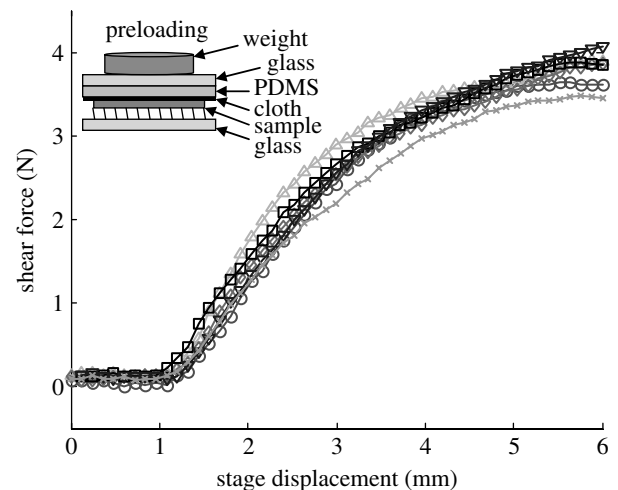
[2]The Tabor parameter (Johnson 1997) was calculated as 1.6 for a 0.3 μm radius fibre tip. This is closer to the JKR region (greater than 3–5) than the DMT region (less than 0.1), and hence the JKR model of contact was used.

Figure 6. Shear force of a 2×1.2 cm^2 microfibre array with different preloads. The sample was preloaded uniformly using a cloth, PDMS, glass and a weight. Preload: circle, 825 mN cm^{-2}; triangle, 416 mN cm^{-2}; diamond, 212 mN cm^{-2}; square, 91 mN cm^{-2}; inverted triangle, 50 mN cm^{-2}; cross, 8 mN cm^{-2}.

the initially straight fibre to have *side contact* (figure 9) with the glass. Side contact gives rise to much larger true contact areas than those predicted for tip contact. We use a side contact model to provide upper bounds on fibre shear force. Previously, the side contact model was used to explain the normal adhesion of carbon nanotubes, silicon nanowires and other high aspect ratio nanoscale fibres (Majidi *et al.* 2005; Majidi 2007). Specifically, side contact is stable when the surface forces exceed the elastic restoring forces in the deformed fibre. Bending is aided by the shear load V applied to individual fibres as the sample is dragged along a substrate.

To model the large deformations required for side contact, the fibres are treated as elastic rods. In their natural (undeformed) configuration, the fibres are straight. During sliding each fibre is loaded by a shear force $V = V_{\text{s}}$. We let $v = v(s)$ denote the lateral deflection of a fibre of length L caused by a shear load V acting on the tip. The coordinate s represents the arc length from the fibre base. The elastica solution corresponds to the function $\phi = \text{d}v/\text{d}s$ that satisfies the ordinary differential equation

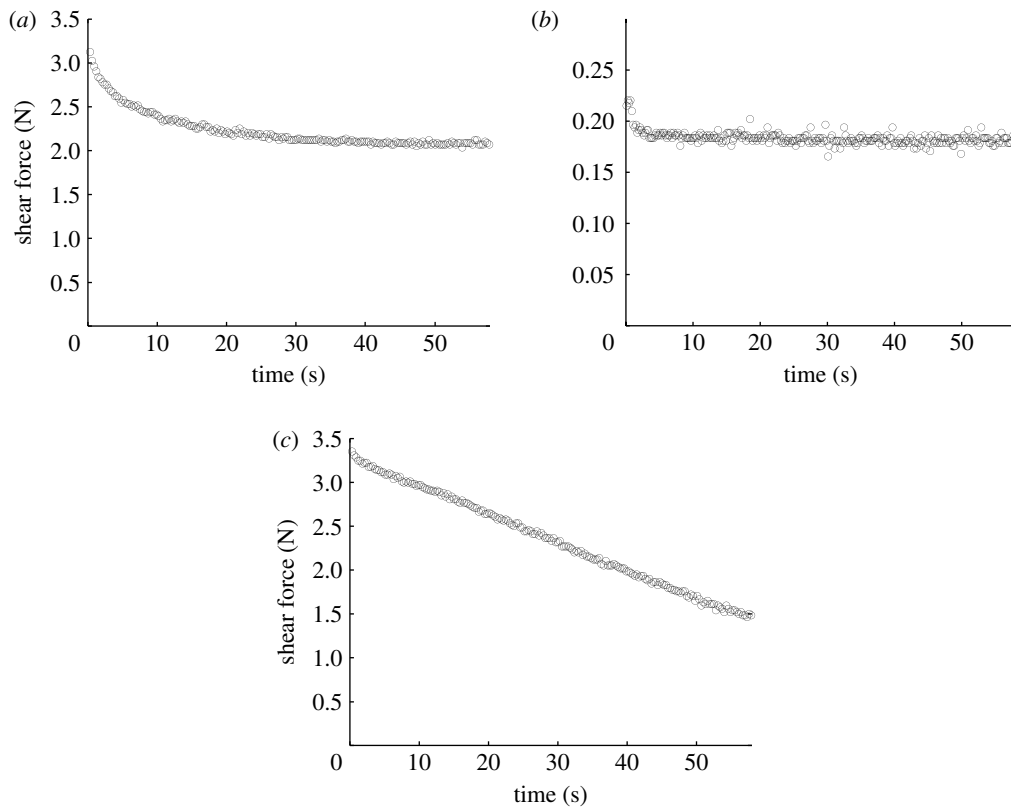$$EI\phi'' + V_{\text{s}} \cos \phi = 0, \qquad (4.1)$$

Figure 7. Comparison of relaxation behaviour of (a) microfibre array, (b) natural gecko setal array and (c) PSA after the stage stopped moving. Shear force of a microfibre array and natural gecko setal array decreased approximately 30 and 20%, respectively, and maintained constant level, while the PSA kept decreasing shear force.

where the prime denotes the derivative with respect to s, E is elastic modulus, and I is cross-sectional moment of inertia.

Letting c denote the length of side contact, it follows that $\phi = \pi/2 \, \forall \, s \in [L-c, L]$. Along the segment $s \in [0, L-c]$, ϕ is the solution to (4.1) along with the boundary conditions $\phi(0) = 0$ and $\phi(L-c) = \pi/2$. The unknown c is determined by the natural boundary condition (Majidi 2007)

$$\frac{1}{2} EI \{\phi'(L-c)\}^2 = \omega, \tag{4.2}$$

where ω is the energy of adhesion per unit length of side contact. From Majidi *et al.* (2005)

$$\omega = 6 \left\{ \frac{(1-\nu^2) r^2 W_{\mathrm{ad}}^4}{\pi E} \right\}^{1/3}. \tag{4.3}$$

Due to surface roughness of the fibre, the actual energy of adhesion per unit length is likely to be significantly lower than predicted (Persson & Gorb 2003). The length of stable side contact c^* is determined numerically by simultaneously solving equations (4.1) and (4.2), for $V = V_m(c)$, where V depends on contact length. The analysis predicts stable side contact under pure shear loading. The length of stable side contact is approximately $c^* = 9.5 \, \mu$m.

We consider two bounds for the maximum shear force, spontaneous fracture of the entire interface (V_1) and elastic peeling (V_2). Both bounds will overestimate shear force, as they ignore surface roughness, and possible interference between fibres or backing membrane buckling.

If sliding occurs only after spontaneous fracture of the entire interface, then the strength of the individual fibre contact will be proportional to the total true area of side contact, cb, where

$$b = 8 \left\{ \frac{(1-\nu^2) r^2 W_{\mathrm{ad}}}{\pi E} \right\}^{1/3} \tag{4.4}$$

is the width of contact (Majidi *et al.* 2005). For the PP microfibre parameters, $b = 74$ nm. Thus, an upper bound on the shear force for a single fibre in side contact is

$$V_1 = \tau cb. \tag{4.5}$$

From the above, the predicted shear force V_1 is 7 μN, greatly exceeding the 210 nN shear force estimated from experiment. (Using 210 nN shear force, the estimated true contact area per fibre is only 2.1×10^{-10} cm^2, and a square centimetre of patch has estimated true contact area of 0.009 cm^2, only 0.9% of the patch area.)

Contact shear failure can also result from the stretching of the fibre on the surface, which corresponds to the elastic term from the Kendall peel model (Kendall 1975) at low peel angle. Converting from the rectangular strip in the Kendall peel model to a cylinder in side contact, we have

$$V_2 = \sqrt{2E\pi r^2 \omega}. \tag{4.6}$$

The upper bound V_2 for low-angle peeling is 970 nN, again greatly exceeding the average experimental value.

As mentioned above, surface roughness of the fibres will reduce the effective work of adhesion, partially explaining the lower measured shear force. In addition,
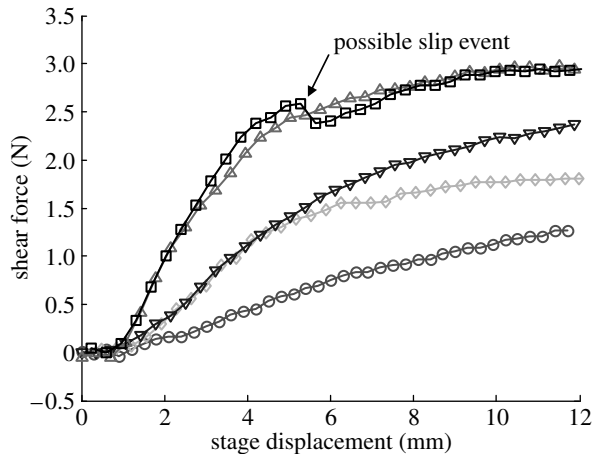
Figure 8. Shear force of a 2×2 cm^2 microfibre array with repeated trials at 5 min intervals after the array had relaxed for 4 days. For the sample, $V_x=120\ \mu\text{m s}^{-1}$. Tests: circle, first; diamond, second; inverted triangle, third; triangle, fourth; square, fifth.

Figure 9. Elastica model of fibre under pure shear loading making side contact with a surface.

the estimated side contact length $c^*=9.5\ \mu\text{m}$ for an isolated fibre is not likely to be achieved in a structure with average fibre-to-fibre spacing of 1.5 μm. Hence, interactions between neighbouring fibres may prevent an average fibre from being in complete side contact.

In contrast to sliding shear force, the tensile pull-off force is quite low, as the fibre will spontaneously transition to tip contact once the shear load is removed. In tip contact, the normal pull-off force is $F_{\text{JKR}}=3/2\pi rW_{\text{ad}}=42$ nN. In pull-off in the normal direction, height variation of the fibres (approx. uniform distribution, 17–20 μm), combined with low vertical compliance in tension, drastically reduces pull-off force (Majidi *et al.* 2006). In contrast, since side contact length c^* is much greater than height variation, the shear force is much less dependent on fibre height variation. Hence the high shear adhesion and low normal adhesion force is consistent with the side contact elastica model.

4.2. Sliding and viscoelastic effects

While the side contact elastica model explains high shear force, it does not directly explain sliding enhanced shear adhesion. When compared with fibre length (20 μm), a long sliding distance (5000 μm) was required to reach maximum shear force (4 N) as shown in figure 3. The long sliding distance required for maximum shear force can be partially explained by a growing estimated contact region being balanced by buckling of the thin PP backing. As shown in image 1 in figure 3a, initially only several points are touching the glass, presumably due to natural curvature of the backing and height variation of fibres. As the array slides, a greater number of fibres are engaging and the backing begins buckling. Thus, estimated contact region and buckled area are competing during sliding, which leads to shear force increasing and then saturating.

In our experiments, the natural gecko patch reached maximum shear force after only 200 μm of sliding, with no normal preload. This is comparable to the $\approx100\ \mu\text{m}$
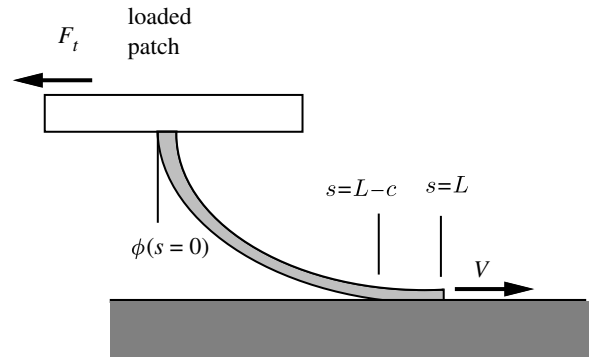
distance seen by Autumn *et al.* (2006*b*), who used a relatively large normal preload of 1 N cm^{-2} before sliding, possibly explaining the shorter distance for full fibre engagement. Although we have no direct observations of estimated contact region for the natural gecko patch during sliding, we speculate that buckling may be less significant. This could be due to the gecko lamellar structure, the patch being mounted to a relatively thick (0.02 cm) acetate strip, as well as the relatively small patch size.

Tests with different dragging velocities on the synthetic and natural patches in figure 5 are consistent with shear force increasing with sliding distance, not on sliding velocity, in the range from 48 to 240 μm s^{-1}. In part II of this paper, Schubert *et al.* (2008) test the velocity range from 5 to 100 μm s^{-1} with similar results. We note that the basic shear force model in equations (4.5) and (4.6) has no velocity dependence, although we cannot rule out velocity dependent effects at higher velocities.

Relaxation tests support that shear adhesion of microfibre arrays does not depend on an internal viscoelastic property of the material, but rather the surface interactions between PP microfibres and glass. In fact, the shear force drop in figure 7a can be explained by a combination of creep relaxation in the force sensor, and sliding of the fibres under tension after stage motion stopped. The force sensor was directly connected to the stage by a string, and stiffness was measured as 4.5×10^3 N m^{-1}. The stage was moved and stopped with the string under tension, and measured force relaxed from 2.79 to 2.58 N. Sliding of the microfibre patch after stopping the stage was approximately 150 μm which corresponds to approximately 0.68 N shear force drop due to sensor and string stiffness. Thus, most of the force drop (approx. 1 N) in figure 7a can be explained by relaxation (0.21 N) of the force sensor/string combination and sliding (0.68 N) of microfibres.

In contrast, the PSA (0.1 cm^2) did not slide on the glass and shear force increased rapidly while the stage moved, but the PSA relaxed slowly after stopping due to viscoelasticity of the soft polymer. In addition, there was much soft polymer residue on the glass after testing with the PSA, which indicates cohesive failure rather than surface sliding between the PSA and glass. After experiments with the PP microfibre array
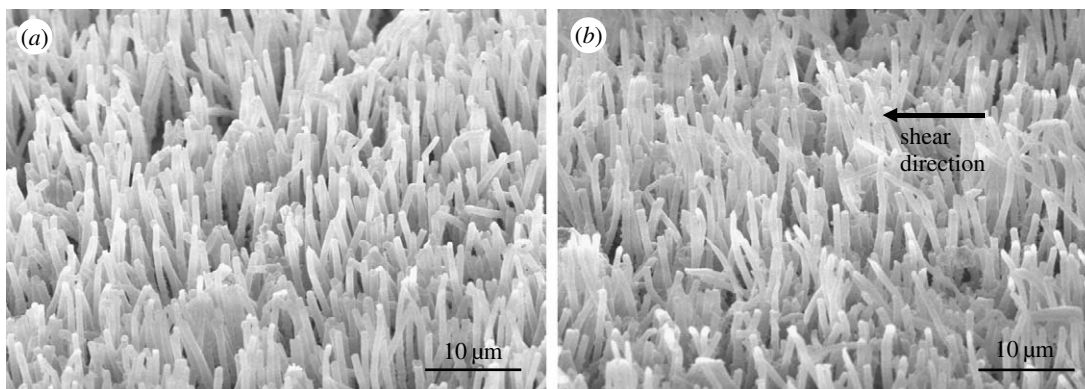
Figure 10. SEM images of microfibres. (*a*) Before testing and (*b*) after shearing more than 50 times. The arrow indicates shearing direction. Only a few fibres show deformation. Images in (*a*,*b*) were taken from different spots.

and natural gecko setal array, no residue was found on the glass. These comparisons support that the viscous deformation typical of detaching PSAs does not seem to occur in the gecko setal array (Gravish *et al.* 2008) or in our microfibre array. Thus, our microfibre array is free from material degradation as opposed to PSAs which lose viscoelastic energy from internal friction processes such as cavitation and fibrillation (Creton & Fabre 2002). The low viscoelastic losses of the PP GSA are consistent with the observation that the microfibre array has high shear adhesion but has low peel strength, as minimal energy is dissipated during peeling.

4.3. Preload independence

Preload was not an important factor for the saturated shear force as shown in figure 6. As shown in the top left image in figure 3, the initial estimated contact region is very small without sliding displacement, even after application and removal of a compressive preload. After the preload is removed, a small number of fibres in a few regions may be adhering to the glass. Higher and lower preloads do not significantly change initial estimated contact region. We observe that a compressive preload apparently flattens the patch uniformly against the surface, removing any initial curvature. The maximum preload of $0.825 \, \mathrm{N \, cm^{-2}}$ is less than the load of $1.6 \, \mathrm{N \, cm^{-2}}$ estimated by Majidi *et al.* (2006) to buckle all fibres, hence not all fibres are making contact with the glass during preload. In addition, the image of the estimated contact region shows no evidence of fibre engagement over the whole patch after preload is removed, which is consistent with the non-adhesive default state of the vertical fibres.

A uniformly increasing estimated region of contact during sliding helps to prevent contact concentrations which can lead to the backing buckling. Thus, slightly touching the samples with a gloved finger was enough preload for high shear adhesion. We note that the fibres are only stably in side contact with a shear load applied; the normal preload will not engage fibres in side contact, and when preload is removed, fibres will return to the default vertical state. Hence, the independence from compressive preload further supports the side contact model.

4.4. Durability

To examine contamination or wear, we took SEM images of an unused (figure 10*a*) and a used sample (figure 10*b*) which was shear-tested more than 50 times. Contamination or obvious wear was not visible, although there are some fibres plastically deformed along the shear direction due to repeated high shear loadings.

Shear adhesion of the samples increased as tests were repeated, as shown in figure 8. Enhanced performance is likely caused by angling of the fibres, which makes the fibres more compliant in the normal direction (Sitti & Fearing 2003) and reduces height variation. Examination with an optical microscope showed that microfibres were angled after repeated testings as shown in figure 11. High shear loading angled some of the fibres (presumably fibres engaged with the surface) but did not angle all fibres uniformly. The angling was not permanent, and fibres recovered to near vertical after several hours when unloaded. Thus, developing a fabrication method for uniformly and permanently angled fibres will be an interesting research topic. Although photolithographic methods have been used to make $25 \, \mu\mathrm{m}$ diameter angled fibres (Aksak *et al.* 2007*a*), the $0.6 \, \mu\mathrm{m}$ fibre diameter used here may be a challenge for lithographic methods.

4.5. Implications for climbing robots and comparison to other GSAs

Pure shear tests at the whole-patch scale showed several properties which are important for climbing robots. The peel strength of $0.15 \, \mathrm{N \, m^{-1}}$ is low enough for easy detachment during vertical running. Shear force increased with sliding distance, which is critical for arresting slip (which could lead to a fall). For both natural and synthetic fibre arrays, shear force recovered after slip events. It is likely that these displacement dependent forces will be important in stabilizing dynamic wall climbers (Autumn *et al.* 2007).

The PP based microfibre array described in this paper has similar stiffness and aspect ratio to natural tokay gecko. Although actual length (approx. $20 \, \mu\mathrm{m}$) and diameter (approx. $0.6 \, \mu\mathrm{m}$) of the PP fibres are less than those of natural tokay gecko's setae, the unbranched PP fibres have very close dimension to
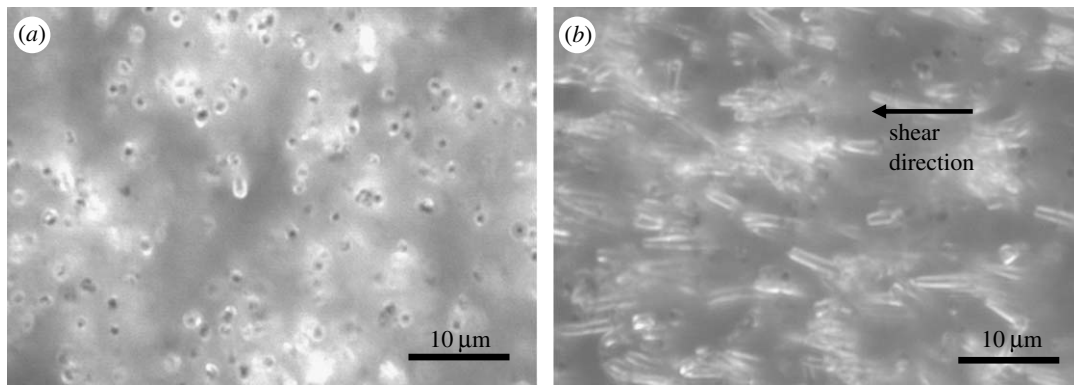
Figure 11. Top view of microfibres through an optical microscope. (*a*) Vertical fibres and (*b*) bent fibres within 10 min after loading with high shear force. The arrow indicates shearing direction. Images in (*a*,*b*) were taken from different spots.

Table 1. Comparison of other adhesives. (PP, polypropylene; PU, polyurethane; PVS, polyvinylsiloxane; MWCNT, multiwalled carbon nanotube.)

	tokay gecko	this paper	Santos *et al.* (2007)	Gorb *et al.* (2007) and Varenberg & Gorb (2007)	Ge *et al.* (2007)	Kim & Sitti (2006)	Kustandi *et al.* (2007)
aspect ratio	25	30	2.63	2.5	50 000	4.4	10
length (µm)/diameter (µm)	100/4	18/0.6	1000/380	100/40	400/0.08	20/4.5	2.5/0.25
material	β-keratin	PP	PU	PVS	MWCNT+PSA	PU	parylene
elastic modulus (GPa)	1.5	1	0.0003	0.003	1000	0.003	2.8
sample area (cm^2)	0.0054	2	4	0.066	0.16	0.03	1
preload pressure (N cm^{-2})	<0.05	<0.1	0.06	0.2	50	12	1
shear stress (N cm^{-2})	55	2	0.3	n.a.	36	n.a.	n.a.
unstructured shear (N cm^{-2})	0	∼0	n.a.	2.27	n.a.	n.a.	n.a.
normal w/o shearing (N cm^{-2})	0	∼0	∼0	6.06	5	18	0.7

natural anolis (approx. 12 µm in length and 0.5 µm in diameter; Ruibal & Ernst 1965). It is expected that the hard material used in the PP microfibre arrays will be important for long-term durability and eventual self-cleaning properties which will be difficult with a softer polymer.

It is worthwhile to compare the performance of the PP microfibre array to other recent work in GSAs as summarized in table 1. A particularly important property for a gecko-like adhesive is that one should be able to obtain a high shear force (useful for climbing) yet a low normal force (for easy detachment). One can note that a conventional PSA can be used to obtain both high shear adhesion and high normal pull-off forces on glass. In addition, a low normal preload is desired for ease of engagement during running. Of the GSAs in table 1, only the reported PP fibre array and the soft polyurethane (PU) structures of Santos *et al.* (2007) show the desirable directional adhesive and low preload properties in a macroscale patch. The PU-based angled stalks with a sharp tip have negligible normal adhesion without shear load even though the material is soft. It is interesting to note that polyvinylsiloxane (PVS)-based mushroom-shaped stalks (Gorb *et al.* 2007; Varenberg & Gorb 2007) have high normal adhesion (6.06 N cm^{-2}) without shear load but become non-adhesive with shear loading because the mushroom-shaped tips rotate away from the contacting surface.

5. CONCLUSION

Gecko-inspired synthetic microfibre arrays were fabricated with a non-tacky stiff polymer. As with natural gecko setal arrays, the fabricated microfibre array shows increasing shear force as a function of sliding distance on smooth glass. This unique property provides stability of the detachable adhesive (robust to a shear disturbance or vibration). Comparisons with PSA supports that shear force from the microfibre array does not depend on viscous creep; thus, low energy detachment is possible. The durable microfibre array was able to hold as great as 4 N in shear with a 2 cm^2 nominal patch area when the array slid 1 cm and had shear stress greater than 9 N cm^{-2} for the estimated contact region, approximately 15% of the natural gecko lamella patch we tested. The high shear adhesion force is due to side contact, which could substitute for complicated spatula structures on smooth surfaces. The PP microfibre array has sufficient shear adhesion for small climbing robots, and has the unique property that performance improves with use, probably due to fibre deformation.

REFERENCES

Aksak, B., Murphy, M. P. & Sitti, M. 2007*a* Adhesion of biologically inspired vertical and angled polymer microfiber arrays. *Langmuir* **23**, 3323–3332. (doi:10.1021/la062697t)

Aksak, B., Sitti, M., Casell, A., Li, J., Meyyappan, M. & Callen, P. 2007*b* Friction of partially embedded vertically aligned carbon nanofibers inside elastomers. *Appl. Phys. Lett.* **91**, 061906. (doi:10.1063/1.2767997)

Antoniou, A. & Bastawros, A. F. 2003 Deformation characteristics of tin-based solder joints. *J. Mater. Res.* **18**, 2304–2310.

Autumn, K. 2007 Gecko adhesion: structure, function, and applications. *MRS Bull.* **32**, 473–478.

Autumn, K. & Gravish, N. 2008 Gecko adhesion: evolutionary nanotechnology. *Phil. Trans. R. Soc. A* **366**, 1575–1590. (doi:10.1098/rsta.2007.2173)

Autumn, K. & Hansen, W. 2006 Ultrahydrophobicity indicates a non-adhesive default state in gecko setae. *J. Comp. Physiol. A* **192**, 1205–1212. (doi:10.1007/s00359-006-0149-y)

Autumn, K., Liang, Y. A., Hsieh, S. T., Zesch, W., Chan, W.-P., Kenny, W. T., Fearing, R. & Full, R. J. 2000 Adhesive force of a single gecko foot-hair. *Nature* **405**, 681–685. (doi:10.1038/35015073)

Autumn, K., Majidi, C., Groff, R. E., Dittmore, A. & Fearing, R. S. 2006*a* Effective elastic modulus of isolated gecko setal arrays. *J. Exp. Biol.* **209**, 3558–3568. (doi:10.1242/jeb.02469)

Autumn, K., Dittmore, A., Santos, D., Spenko, M. & Cutkosky, M. 2006*b* Frictional adhesion: a new angle on gecko attachment. *J. Exp. Biol.* **209**, 3569–3579. (doi:10.1242/jeb.02486)

Autumn, K., Hsieh, S. T., Dudek, D. M., Chen, J., Chitaphan, C. & Full, R. J. 2007 Dynamics of geckos running vertically. *J. Exp. Biol.* **209**, 206–272.

Creton, C. & Fabre, P. 2002 Tack. In *Adhesion science and engineering*, vol. 1 (eds A. V. Pocius, D. A. Dillard & M. Chaudhury). The mechanics of adhesion, pp. 535–576. Amsterdam, The Netherlands: Elsevier.

Ge, L., Sethi, S., Ci, L., Ajayan, P. M. & Dhinojwala, A. 2007 Carbon nanotube-based synthetic gecko tapes. *Proc. Natl Acad. Sci. USA* **104**, 10 792–10 795. (doi:10.1073/pnas.0703505104)

Geim, A. K., Dubonos, S. V., Grigorieva, I. V., Novoselov, K. S., Zhukov, A. A. & Shapoval, S. Yu. 2003 Microfabricated adhesive mimicking gecko foot-hair. *Nat. Mater.* **2**, 461–463. (doi:10.1038/nmat917)

Gorb, S., Varenberg, M., Peressadko, A. & Tuma, J. 2007 Biomimetic mushroom-shaped fibrillar adhesive microstructure. *J. R. Soc. Interface* **4**, 271–275. (doi:10.1098/rsif.2006.0164)

Gracias, D. H. & Somorjai, G. A. 1998 Continuum force microscopy study of the elastic modulus, hardness and friction of polyethylene and polypropylene surfaces. *Macromolecules* **31**, 1269–1276. (doi:10.1021/ma970683b)

Gravish, N., Wilkinson, M. & Autumn, K. 2008 Frictional and elastic energy in gecko adhesive detachment. *J. R. Soc. Interface.* **5**, 339–348. (doi:10.1098/rsif.2007.1077)

Johnson, K. L. 1997 Adhesion and friction between a smooth elastic spherical asperity and a plane surface. *Proc. R. Soc. A* **453**, 163–179. (doi:10.1098/rspa.1997.0010)

Johnson, K. L., Kendall, K. & Roberts, A. D. 1971 Surface energy and the contact of elastic solids. *Proc. R. Soc. A* **324**, 301–313. (doi:10.1098/rspa.1971.0141)

Kendall, K. 1975 Thin-film peeling—the elastic term. *J. Phys. D. Appl. Phys.* **8**, 1449–1452. (doi:10.1088/0022-3727/8/13/005)

Kim, S. & Sitti, M. 2006 Biologically inspired polymer microfibers with spatulate tips as repeatable fibrillar adhesives. *Appl. Phys. Lett.* **89**, 261911. (doi:10.1063/1.2424442)

Kustandi, T. S., Samper, V. D., Yi, D. K., Ng, W. S., Neuzil, P. & Sun, W. 2007 Self-assembled nanoparticles based fabrication of gecko foot-hair-inspired polymer nanofibers. *Adv. Funct. Mater.* **17**, 2211–2218. (doi:10.1002/adfm.200600564)

Majidi, C. 2007 Remarks on formulating an adhesion problem using Euler's elastica. *Mech. Res. Commun.* **34**, 85–90. (doi:10.1016/j.mechrescom.2006.06.007)

Majidi, C., Groff, R. E. & Fearing, R. S. 2005 Attachment of fiber array adhesive through side contact. *J. Appl. Phys.* **98**, 103521. (doi:10.1063/1.2128697)

Majidi, C. *et al.* 2006 High friction from a stiff polymer using micro-fiber arrays. *Phys. Rev. Lett.* **97**, 076103. (doi:10.1103/PhysRevLett.97.076103)

Peattie, A. M., Majidi, C., Corder, A. & Full, R. J. 2007 Ancestrally high elastic modulus of gecko setal β-keratin. *J. R. Soc. Interface* **4**, 1071–1076. (doi:10.1098/rsif.2007.0226)

Persson, B. N. J. & Gorb, S. 2003 The effect of surface roughness on the adhesion of elastic plates with applications to biological systems. *J. Chem. Phys.* **119**, 11 437–11 444. (doi:10.1063/1.1621854)

Pooley, C. M. & Tabor, D. 1972 Friction and molecular structure: the behaviour of some thermoplastics. *Proc. R. Soc. A* **329**, 251–274. (doi:10.1098/rspa.1972.0112)

Ruibal, R. & Ernst, V. 1965 The structure of the digital setae of lizards. *J. Morphol.* **117**, 271–294. (doi:10.1002/jmor.1051170302)

Santos, D., Kim, S., Spenko, M., Parness, A. & Cutkosky, M. 2007 Directional adhesive structures for controlled climbing on smooth vertical surfaces. In *Proc. IEEE ICRA*, pp. 1262–1267.

Schubert, B., Majidi, C., Groff, S., Baek, S., Bush, B., Maboudian, R. & Fearing, R. S. 2007 Towards friction and adhesion from high modulus microfiber arrays. *J. Adhes. Sci. Technol.* **21**, 1297–1315. (doi:10.1163/156856107782328344)

Schubert, B., Lee, J., Majidi, C. & Fearing, R. S. 2008 Sliding-induced adhesion of stiff polymer microfibre arrays. II. Microscale behaviour. *J. R. Soc. Interface* **5**, 845–853. (doi:10.1098/rsif.2007.1309)

Sitti, M. & Fearing, R. S. 2003 Synthetic gecko foot-hair micro/nano-structures as dry adhesives. *J. Adhes. Sci. Technol.* **18**, 1055–1074. (doi:10.1163/156856103322113788)

Varenberg, M. & Gorb, S. 2007 Shearing of fibrillar adhesive microstructure: friction and shear-related changes in pull-off force. *J. R. Soc. Interface* **4**, 721–725. (doi:10.1098/rsif.2007.0222)

Zhao, Y., Tong, T., Delzeit, L., Kashani, A., Meyyappan, M. & Majumdar, A. 2006 Interfacial energy and strength of multiwalled-carbon-nanotube-based dry adhesive. *J. Vac. Sci. Technol. B* **24**, 331–335. (doi:10.1116/1.2163891)